

# Au+Au central collisions at 150, 250 and 400 AMeV energies in QMD with relativistic forces

J. Németh <sup>a</sup>, G. Papp <sup>a,b,c</sup> and H. Feldmeier <sup>b</sup>

<sup>a</sup>*Institute for Theoretical Physics, Eötvös Univ., H-1088 Budapest, Hungary,*

<sup>b</sup>*Gesellschaft für Schwerionenforschung, D-64220, Darmstadt, Germany,*

<sup>c</sup>*ITP, Univ. Heidelberg, Philosophenweg 19, D-69120 Germany.*

---

## Abstract

An extensive comparison of the recent experimental data published by the FOPI collaboration at GSI with the results of a relativistically covariant formulation of a QMD code is presented. For most of the quantities we find agreement with the experimental results showing that the derived force has a reasonable momentum dependence.

*PACS:* 25.70Mn, 25.75.+r

*Keywords:* Molecular Dynamics; Relativistic forces.

---

## 1 Introduction

The new experimental facilities [3] are able measure the momenta of the protons and clusters and their charge which are created in heavy ion collisions at intermediate energies (100 AMeV – 2 AGeV) in an exclusive way. Event-by-event analysis allows to test molecular dynamical models with respect to the degree of equilibration, flow and cluster formation. Consequently, the existing models are forced to reproduce not only one-body observables, which are mainly governed by the mean-field and the continuity equation but also many-body correlations which are necessary to create intermediate mass fragments (IMF) at low excitation energy.

Nowadays it is popular to describe heavy ion collisions with the help of transport models like BUU [4], QMD [5,6], etc. In these models the interaction is divided into two parts, a smooth mean-field and a random collision term. The mean-field force is often treated non-relativistically and the elastic two-particle

collision cross section is determined from the free nucleon-nucleon scattering. However, at beam energies above 500 AMeV a relativistic treatment is necessary. Since it has been recognized, that at least up to 2 AGeV the mean-field is still of importance, one should include it in a relativistically invariant form. At these energies particle creation in a hadronic medium is the important issue. In order to disentangle the effect of the mean-field from the medium dependence of the cross-sections one should try to check the validity of the applied mean-field at lower energies, where particle creation is negligible.

In a previous publication by the authors [2] a QMD code was developed in which the mean-field dynamics was based on a relativistic lagrangian of the Walecka type. A covariant many-body Lagrange function for point-like particles with scalar and vector two-body potentials was derived, which still had the saturation property of the original Walecka-type lagrangian. We checked this code at low energies (50 – 200 AMeV) in O–Br collisions and found, as many authors before, that the Walecka type of mean-field force is not satisfactory for QMD calculations due to the large values of the scalar and vector coupling. Instead of adding third and fourth powers of scalar field in the lagrangian [7] we used a derivative coupling proposed first by Zimányi and Moszkowski (ZM) [8]. The advantage of this lagrangian is that the coupling constant determined by fitting nuclear saturation density and energy are much smaller than for a linear coupling of the scalar field. In addition the resulting incompressibility is two times smaller (see Table 1).

In this paper we deduce a relativistically invariant formulation of the mean-field forces starting from the ZM lagrangian and using the small acceleration approximation. We use the derived forces to investigate central gold on gold collisions at 150, 250 and 400 AMeV and compare our results with the FOPI experiments [1]. We also determined the freeze out density and time as the function of the energy. In the following we use  $\hbar = c = 1$  units, except where they are indicated explicitly.

The paper is organized as follows. In Section 2 the relativistic equations of motions for the nucleons are derived generalizing the results of the previous paper [2]. Section 3 gives details of the QMD calculations. In Section 4 we compare our results with the experimental data and in Section 5 the freeze out time and density are determined. In Section 6 the distribution of intermediate mass fragments and their dependence on various parameters is analyzed. Finally we conclude in Section 7.

## 2 Relativistic equations of motion for nucleons

In this section we are sketching the derivation of the relativistic equations of motion for the 4-positions and 4-momenta of the nucleons [2,?,9]. We start from a field theoretical lagrangian which includes besides a scalar field  $\phi(x)$  and a vector field  $A_\alpha(x)$  an iso-vector vector field  $\vec{B}_\alpha(x)$ ,

$$\begin{aligned} \mathcal{L}(x) = & \bar{\psi}(x) \left( \gamma^\alpha i \partial_\alpha - m f(\phi(x)) \right) \psi(x) \\ & - g_\omega \bar{\psi}(x) \gamma^\alpha \psi(x) A_\alpha(x) - g_\rho \bar{\psi}(x) \gamma^\alpha \frac{1}{2} \vec{\tau} \psi(x) \vec{B}_\alpha(x) \\ & - \frac{1}{2} \phi(x) (\partial_\alpha \partial^\alpha + \mu_\sigma^2) \phi(x) \\ & + \frac{1}{2} A^\alpha(x) (\partial_\beta \partial^\beta + \mu_\omega^2) A_\alpha(x) + \frac{1}{2} \partial^\alpha A_\alpha(x) \partial^\beta A_\beta(x) \\ & + \frac{1}{2} \vec{B}^\alpha(x) (\partial_\beta \partial^\beta + \mu_\rho^2) \vec{B}_\alpha(x) + \frac{1}{2} \partial^\alpha \vec{B}_\alpha(x) \partial^\beta \vec{B}_\beta(x) . \end{aligned} \quad (1)$$

In order to avoid the stiff equation of state which results from a linear coupling to the scalar field we use the proposal of Zimányi and Moszkowski [8] to couple the scalar field in a non-linear fashion as

$$f(\phi) = \frac{1}{1 + \frac{g_\sigma}{m} \phi} . \quad (2)$$

The field equations are

$$\left\{ \gamma_\alpha (i \partial_\alpha - g_\omega A_\alpha(x) - g_\rho \frac{1}{2} \vec{\tau} \vec{B}_\alpha(x)) - m f(\phi(x)) \right\} \psi(x) = 0 \quad (3)$$

for the nucleons,

$$(\partial^\beta \partial_\beta + \mu_\sigma^2) \phi(x) = -m f'(\phi(x)) \bar{\psi}(x) \psi(x) \quad (4)$$

for the scalar field with  $f' = df/d\phi$  and

$$\begin{aligned} (\partial^\beta \partial_\beta + \mu_\omega^2) A^\alpha(x) &= \partial^\alpha \partial_\beta A^\beta(x) + g_\omega \bar{\psi}(x) \gamma^\alpha \psi(x) \\ (\partial^\beta \partial_\beta + \mu_\rho^2) \vec{B}^\alpha(x) &= \partial^\alpha \partial_\beta \vec{B}^\beta(x) + g_\rho \bar{\psi}(x) \gamma^\alpha \frac{1}{2} \vec{\tau} \psi(x) \end{aligned} \quad (5)$$

for the vector fields.

In the mean-field approximation the source terms are replaced by their expectation values  $\langle \bar{\psi}(x)\psi(x) \rangle$ ,  $\langle \bar{\psi}(x)\gamma^\alpha\psi(x) \rangle$  and  $\langle \bar{\psi}(x)\gamma^\alpha\vec{\tau}\psi(x) \rangle$ , so that the scalar and vector fields become classical fields.

In addition we do not allow isospin rotations but conserve neutron and proton currents individually. This means for the isospin components

$$\langle \bar{\psi}(x)\gamma^\alpha\vec{\tau}\psi(x) \rangle = \begin{pmatrix} j_p^\alpha(x) - j_n^\alpha(x) \\ 0 \\ 0 \end{pmatrix} \quad (6)$$

with

$$\partial_\alpha j_p^\alpha(x) = 0 \quad \text{and} \quad \partial_\alpha j_n^\alpha(x) = 0. \quad (7)$$

Here  $j_p^\alpha(x)$  denotes the proton current and  $j_n^\alpha(x)$  the neutron current. Since the baryon current

$$\langle \bar{\psi}(x)\gamma^\alpha\psi(x) \rangle = j^\alpha(x) = j_p^\alpha(x) + j_n^\alpha(x) \quad (8)$$

is also conserved, the four-divergence of both classical fields, the isoscalar  $A^\alpha(x)$  and the isovector  $\vec{B}^\alpha(x)$  vanish. Therefore the terms  $\partial^\alpha\partial_\beta A^\beta(x)$  and  $\partial^\alpha\partial_\beta \vec{B}^\beta(x)$  can be omitted in Eq. (5).

As we are using the relativistic scalar and vector fields only for the mean-field part of the nuclear interaction we follow the suggestion [?,9] to exclude radiation of mesonic fields from the very beginning by using the action-at-a-distance formulation with the symmetric Green's function of Wheeler and Feynman [10],

$$G(x-y) = \frac{1}{2} \left( G^{advanced}(x-y) + G^{retarded}(x-y) \right). \quad (9)$$

Then the formal solutions of the Eq. (4)

$$\phi(x) = -m \int d^4y \ G_\sigma(x-y) f'(\phi(y)) \langle \bar{\psi}(y)\psi(y) \rangle \quad (10)$$

and of Eqs. (5)

$$\begin{aligned} A^\alpha(x) &= g_\omega \int d^4y \ G_\omega(x-y) \langle \bar{\psi}(y)\gamma^\alpha\psi(y) \rangle \\ \vec{B}^\alpha(x) &= \frac{1}{2} g_\rho \int d^4y \ G_\rho(x-y) \langle \bar{\psi}(y)\gamma^\alpha\vec{\tau}\psi(y) \rangle \end{aligned} \quad (11)$$

fulfill the desired boundary condition of vanishing incoming and outgoing free fields.

Eliminating the fields from the lagrangian (1) leads to the non-local action which contains only nucleon variables:

$$\begin{aligned} \int d^4x \mathcal{L}(x) = & \int d^4x \langle \bar{\psi}(x) \gamma^\alpha i \partial_\alpha \psi(x) \rangle \\ & - \int d^4x m \left[ f(\phi(x)) - \frac{1}{2} \phi(x) f'(\phi(x)) \right] \langle \bar{\psi}(x) \psi(x) \rangle \\ & - \frac{1}{2} g_\omega^2 \int d^4x d^4y \langle \bar{\psi}(x) \gamma^\alpha \psi(x) \rangle G_\omega(x-y) \langle \bar{\psi}(y) \gamma_\alpha \psi(y) \rangle \\ & - \frac{1}{2} g_\rho^2 \int d^4x d^4y \langle \bar{\psi}(x) \gamma^\alpha \frac{1}{2} \vec{\tau} \psi(x) \rangle G_\rho(x-y) \langle \bar{\psi}(y) \gamma_\alpha \frac{1}{2} \vec{\tau} \psi(y) \rangle \end{aligned} \quad (12)$$

where  $\phi(x)$  is given in terms of  $\langle \bar{\psi}(x) \psi(x) \rangle$  by the integral equation (10). If quantum effects are negligible the scalar density and vector current density can be represented in terms of the world lines of the nucleons as

$$\rho_\sigma(x) := \langle \bar{\psi}(x) \psi(x) \rangle \rightarrow \sum_{j=1}^A \int d\theta_j \delta^4(x - r_j(\theta_j)) \quad (13)$$

$$j^\mu(x) := \langle \bar{\psi}(x) \gamma^\mu \psi(x) \rangle \rightarrow \sum_{j=1}^A \int d\theta_j \delta^4(x - r_j(\theta_j)) u_j^\mu(\theta_j), \quad (14)$$

$$\vec{i}^\mu(x) := \langle \bar{\psi}(x) \gamma^\mu \vec{\tau} \psi(x) \rangle \rightarrow \sum_{j=1}^A \int d\theta_j \delta^4(x - r_j(\theta_j)) u_j^\mu(\theta_j) \vec{\tau}_j, \quad (15)$$

where  $r_j(\theta_j)$  denotes the world line of the nucleon  $j$  at its proper time  $\theta_j$  and  $u_j(\theta_j)$  its 4-velocity. Furthermore  $\vec{\tau}_j$  denotes twice the isospin of the nucleon  $j$ . Since there is no exchange of charged mesons in this lagrangian the isospin direction does not change in time so that  $\langle \text{neutron} | \vec{\tau} | \text{neutron} \rangle \equiv \vec{\tau}_{\text{neutron}} = (-1, 0, 0)$  and  $\langle \text{proton} | \vec{\tau} | \text{proton} \rangle \equiv \vec{\tau}_{\text{proton}} = (1, 0, 0)$ . This implies that only the first component of the iso-vector current  $\vec{i}^\mu(x)$  and the iso-vector field  $\vec{B}^\mu(x)$  contribute. Therefore we shall simply write  $i^\mu(x)$  and  $B^\mu(x)$ , respectively.

Nucleons in nuclei can however not be localized well enough for treating them as classical particles on world lines. The Fermi momentum sets a lower limit to the size of the nucleon wave packet in coordinate space which is of the order of 2 fm. These effects, the Pauli principle and other quantum effects, are properly taken care of in Antisymmetrized Molecular Dynamics (AMD) [11] and in Fermionic Molecular Dynamics (FMD) [12]. However, presently neither the AMD nor the FMD equations of motion can be solved numerically for large systems like gold on gold. Therefore, we mimic the finite size effect of the wave packets by folding the finally obtained forces with Gaussian density

distributions for the nucleons. This "smearing" provides also the prescription how to eliminate strong forces at short distances which are taken care of by the random forces of the collision term.

Therefore, the forces to be derived in the following are only meant to represent the long range part of the nuclear interactions which constitute a mean field. In this sense  $r_j(\theta_j)$  is the mean world line of the nucleon and  $u_j(\theta_j)$  its mean 4-velocity.

Using the representation (14) the isoscalar field at a space-time point  $x$ , for example, is given by integrals over past and future proper times  $\theta_j$  as

$$B^\alpha(x) = g_\rho \sum_{j=1}^A \int d\theta_j G_\rho(x - r_j(\theta_j)) u_j^\alpha(\theta_j) \frac{1}{2} \tau_j . \quad (16)$$

By identifying the different contribution of the action (12) with their representation in terms of mean positions and mean momenta of the nucleons one obtains the non-instantaneous action-at-a-distance [10]:

$$\begin{aligned} \int d^4x \mathcal{L}(x) \rightarrow \\ \mathcal{A} = & -\frac{1}{2} \sum_{i=1}^A \int d\theta_i m_i^*(\theta_i) u_i(\theta_i)^2 \\ & - m \sum_{i=1}^A \int d\theta_i \left[ f(\phi(r_i(\theta_i))) - \frac{1}{2} \phi(r_i(\theta_i)) f'(\phi(r_i(\theta_i))) \right] \\ & - \frac{1}{2} g_\omega^2 \sum_{i,j=1}^A' \int d\theta_i d\theta_j G_\omega(r_i(\theta_i) - r_j(\theta_j)) u_{i\alpha}(\theta_i) u_j^\alpha(\theta_j) \\ & - \frac{1}{2} g_\rho^2 \sum_{i,j=1}^A' \int d\theta_i d\theta_j G_\rho(r_i(\theta_i) - r_j(\theta_j)) u_{i\alpha}(\theta_i) u_j^\alpha(\theta_j) \frac{1}{2} \vec{\tau}_i \frac{1}{2} \vec{\tau}_j , \end{aligned} \quad (17)$$

where the prime on the sum means  $i \neq j$ .

In this non-local Lagrange function the world lines  $r_i(\theta_i)$  of the particles are the variables. But only three components are independent because the proper time  $\theta$  relates the time to the space component, or the square of the four-velocity equals one ( $(dr/d\theta)^2 = u^2 = 1$ ). Since we want manifest covariant equations of motion Lagrange multipliers  $m_i^*(\theta_i)$  are introduced in (17) and all four components of  $r_i$  are varied.

The result of the variation is

$$\begin{aligned}
\delta\mathcal{A} = & -\sum_{i=1}^A \int d\theta_i m_i^*(\theta_i) u_i^\alpha(\theta_i) \frac{d}{d\theta_i} \delta r_{i\alpha}(\theta_i) \\
& - \frac{1}{2} m \sum_{i=1}^A \int d\theta_i [f'(\phi_i) \delta\phi_i - \phi_i \delta f'(\phi_i)] \\
& - g_\omega^2 \sum_{i,j=1}^A \int d\theta_i d\theta_j \left[ \partial^\alpha G_\omega^{ij} \delta r_{i\alpha}(\theta_i) u_{i\beta}(\theta_i) u_j^\beta(\theta_j) + G_\omega^{ij} \left( \frac{d}{d\theta_i} \delta r_{i\alpha}(\theta_i) \right) u_j^\alpha(\theta_j) \right] \\
& - g_\rho^2 \sum_{i,j=1}^A \int d\theta_i d\theta_j \left[ \partial^\alpha G_\rho^{ij} \delta r_{i\alpha}(\theta_i) u_{i\beta}(\theta_i) u_j^\beta(\theta_j) + G_\rho^{ij} \left( \frac{d}{d\theta_i} \delta r_{i\alpha}(\theta_i) \right) u_j^\alpha(\theta_j) \right] \frac{1}{2} \vec{\tau}_i \frac{1}{2} \vec{\tau}_j
\end{aligned} \tag{18}$$

where  $G^{ij} \equiv G(r_i(\theta_i) - r_j(\theta_j))$  and  $\phi_i \equiv \phi(r_i(\theta_i))$ .

The variation of the part containing the scalar field will be treated below in more detail, as it is not straightforward due to the non-linear coupling and the implicit integral equation (10). According to (10) and (13) the scalar field at 4-position  $r_i$  is given by

$$\phi_i \equiv \phi(r_i) = -m \sum_{i=1}^A \int d\theta_j G_\sigma^{ij} f'(\phi_j) \tag{19}$$

and the variation

$$\delta\phi_i = -m \sum_{j=1}^A \int d\theta_j \left[ \delta G_\sigma^{ij} f'(\phi_j) + G_\sigma^{ij} \delta f'(\phi_j) \right]. \tag{20}$$

Inserting this into the second line of Eq. (18) yields

$$\begin{aligned}
\delta\mathcal{A}_\phi = & \frac{m^2}{2} \sum_{i,j=1}^A \int d\theta_i d\theta_j f'(\phi_i) \delta G_\sigma^{ij} f'(\phi_j) \\
& + \frac{m^2}{2} \sum_{i,j=1}^A \int d\theta_i d\theta_j \left[ f'(\phi_i) G_\sigma^{ij} \delta f'(\phi_j) - \delta f'(\phi_i) G_\sigma^{ij} f'(\phi_j) \right].
\end{aligned} \tag{21}$$

Since  $G_\sigma^{ij} = G_\sigma^{ji}$  is symmetric the last line vanishes and

$$\delta G^{ij} = \partial^\alpha G(r_i - r_j) (\delta r_{i\alpha} - \delta r_{j\alpha}). \tag{22}$$

Integrating those terms which contain proper time derivatives  $d\delta r/d\theta$  by parts and requiring that  $\delta\mathcal{A} = 0$  for arbitrary  $\delta r_i(\theta_i)$  finally yields

$$\begin{aligned} \frac{d}{d\theta} \left( m_i^*(\theta) u_i^\alpha \right) &= m f'(\phi_i) \partial^\alpha \phi_i + g_\omega \left( \partial^\alpha A^\beta(r_i) - \partial^\beta A^\alpha(r_i) \right) u_{i\beta} \\ &\quad + g_\rho \tau_i \left( \partial^\alpha B^\beta(r_i) - \partial^\beta B^\alpha(r_i) \right) u_{i\beta}, \end{aligned} \quad (23)$$

where the fields are given according to Eqs. (10) – (12) by

$$\phi(r_i) = -m \sum_{j \neq i}^A \int d\theta_j G_\sigma^{ij} f'(\phi(r_j)), \quad (24)$$

$$A^\beta(r_i) = g_\omega \sum_{j \neq i}^A \int d\theta_j G_\omega^{ij} u_j^\beta, \quad (25)$$

$$B^\beta(r_i) = g_\rho \sum_{j \neq i}^A \int d\theta_j G_\rho^{ij} u_j^\beta \frac{1}{2} \tau_j \quad (26)$$

and

$$u_i(\theta) = \frac{d}{d\theta} r_i(\theta). \quad (27)$$

The Lagrange parameters  $m_i^*(\theta)$  are determined by multiplying the above equation with  $u_{i\alpha}(\theta)$  and using  $du_i^2/d\theta = 0$ ,

$$\begin{aligned} \frac{dm_i^*(\theta)}{d\theta} &= m f'(\phi(r_i)) \partial^\alpha \phi(r_i) u_{i\alpha} \\ &= m f'(\phi(r_i)) \frac{d}{d\theta} \phi(r_i) = m \frac{d}{d\theta} f(\phi(r_i)), \end{aligned} \quad (28)$$

or

$$m_i^*(\theta) = m f(\phi(r_i)) = \frac{m}{1 + \frac{g_\sigma}{m} \phi(r_i(\theta))}, \quad (29)$$

where the integration constant has been set to zero so that for  $g_\sigma = 0$ ,  $m_i^* = m$ . Each particle has an effective mass  $m_i^*$  which depends through the scalar field  $\phi(r_i(\theta))$  on all other particles in the same way as in the original field-theory Lagrangian.

These derivations led us from a covariant Lagrangian for fields to the following manifestly covariant equations of motion for worldlines,

$$\begin{aligned} m f(\phi(r_i)) \frac{du_i^\alpha}{d\theta} &= m f'(\phi(r_i)) \left( \partial^\alpha \phi(r_i) - \partial^\beta \phi(r_i) u_{i\beta} u_i^\alpha \right) \\ &\quad + g_\omega \left( \partial^\alpha A^\beta(r_i) - \partial^\beta A^\alpha(r_i) \right) u_{i\beta} + g_\rho \vec{\tau}_i \left( \partial^\alpha \vec{B}^\beta(r_i) - \partial^\beta \vec{B}^\alpha(r_i) \right) u_{i\beta}. \end{aligned} \quad (30)$$

The coupling  $mf'(\phi)$  in front of the derivatives of the scalar field always depends on the field itself (which can actually also be chosen different from (29), see [13]),

$$mf'(\phi) = -g_\sigma \left( \frac{m^*(\phi)}{m} \right)^2, \quad (31)$$

the larger the field  $\phi$  the weaker is the coupling.

The equations of motion which result from the Wheeler-Feynman action extended by scalar fields which couple in a non-linear fashion are completely equivalent to the classical field equations, provided the system does not radiate. The reasoning is the same as given by Wheeler and Feynman in [10] for the case of electrodynamics.

However, the Wheeler Feynman equations of motion cannot be solved in general as one needs to know the world lines for all past and future times in order to calculate the fields which enter the equations for the world lines [14]. Furthermore, the no-interaction theorem states that, except in the case of non-interacting particles, there exist no covariant equations of motion for world lines in which only the 4-positions and the 4-velocities at a given time enter, as it is the case in non-relativistic mechanics.

In the following this no-interaction theorem is circumvented by introducing an approximative solution to the non-local Wheeler Feynman equations of motion. This is achieved by the so called small acceleration approximation which does not assume small velocities.

## 2.1 Action-at-a-distance in the small acceleration approximation

In order to conserve manifest covariance of the equations of motion we introduce first the concept of a scalar time. For that the whole Minkowski space is chronologically ordered by a set of space-like surfaces  $S(x)$  which attribute to each 4-position  $x$  a scalar time  $t$  by

$$S(x) = t \quad , \quad \text{with} \quad \partial^0 S(x) > 0. \quad (32)$$

The simplest choice for these isochrones, which we shall use in the following, is  $S(x) = \eta_\alpha x^a$ , where  $\eta_\alpha$  is a position independent time-like 4-vector.

Unlike in a collision the nucleons are not strongly accelerated by the action of the mean-field. Therefore, in order to describe the motion in the mean-

field one may expand each world line around the proper time  $\theta_j^s$  at which the particle is at a given isochrone, i.e.  $t = S(r_j(\theta_j^s))$  for each  $j$ .

$$r_j^\alpha(\theta_j) = r_j^\alpha(\theta_j^s) + (\theta_j - \theta_j^s)u_j^\alpha(\theta_j^s) + \frac{1}{2}(\theta_j - \theta_j^s)^2 a_j^\alpha(\theta_j^s) + \dots . \quad (33)$$

This way we are defining a synchronization prescription for all particles, which does not depend on the frame. For calculating the fields we neglect the quadratic term with the acceleration  $a_j^\alpha(\theta_j^s)$  and all higher powers which leaves us with a straight world line in the vicinity of the synchronizing time  $t = S(r_j(\theta_j^s))$  (c.f. Fig. 1). This is called "small acceleration approximation".

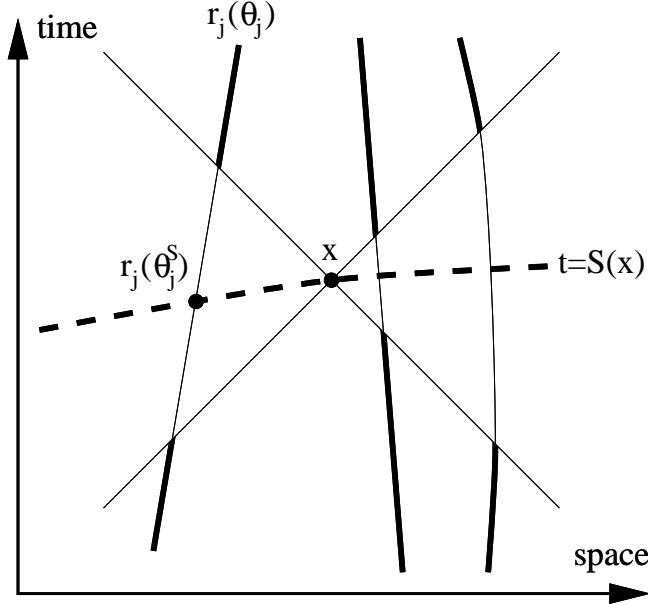


Fig. 1. World lines and synchronizing hypersurface  $S(x)$

The small acceleration approximation is of course best in the vicinity of  $r_j^\alpha(\theta_j^s)$  and becomes worse further away. As sketched in Fig. 1, only those parts of the world lines (thick lines), which are inside the light cone (centered at  $x$ ), contribute to the field strength at point  $x$ . A world line which hits the light cone far away from  $x$  may be badly approximated by Eq. (33), but for short range interactions a distant particle does not contribute anymore to the field at  $x$ .

Thus, the first condition for the validity of the approximation is that the range  $\mu^{-1}$  is small compared to the curvature of the world lines, i.e. the inverse of the acceleration. The second condition is weak radiation, which is fulfilled when the acceleration is small compared to the meson mass  $\mu$ . Both conditions are actually the same, namely

$$| a_\mu a^\mu | \ll \mu^2. \quad (34)$$

The assumption of small acceleration is justified if the  $\phi$ ,  $A^\alpha$  and  $B^\alpha$  fields are only meant to be the mean-field part of the nucleon-nucleon interaction in a hadronic surrounding. The hard collisions between individual nucleons which are due to the repulsive core will cause large accelerations and also create new particles. These hard collisions cannot be described within mean-field models of the Walecka type. Therefore, it is consistent to regard  $\phi(x)$ ,  $A^\alpha(x)$  and  $B^\alpha$  as Hartree mean-fields which bring about only small accelerations and which are not radiated away from their sources.

Inserting the straight world line into Eq. (16) results in the easily understood situation that the field at a point  $x$  is just the sum of Lorentz-boosted Yukawa potentials which are traveling along with the source:

$$B^\alpha(x) = \frac{g_\rho}{4\pi} \sum_j \frac{\exp\left\{-\mu_\rho \sqrt{R_j(x)^2}\right\}}{\sqrt{R_j(x)^2}} u_j^\alpha(\theta_j^s) \frac{1}{2} \tau_j , \quad (35)$$

where  $R_j(x)^2$  is given by

$$R_j(x)^2 = -(x - r_j(\theta_j^s))^2 + \left[ (x^\alpha - r_j^\alpha(\theta_j^s)) u_{j\alpha}(\theta_j^s) \right]^2 . \quad (36)$$

The vector field is derived in an analogue fashion as

$$A^\alpha(x) = \frac{g_\omega}{4\pi} \sum_j \frac{\exp\left\{-\mu_\omega \sqrt{R_j(x)^2}\right\}}{\sqrt{R_j(x)^2}} u_j^\alpha(\theta_j^s) . \quad (37)$$

The scalar field results from the implicit Eq. (24) in which we assume that the scalar field does not vary much along the part of the world line which contributes, *i.e.*  $\phi(r_j(\theta_j)) \approx \phi(r_j(\theta_j^s))$  and hence can be replaced by the field at the synchronizing time. The result is

$$\phi(x) = \frac{g_\sigma}{4\pi} \sum_j \frac{\exp\left\{-\mu_\sigma \sqrt{R_j(x)^2}\right\}}{\sqrt{R_j(x)^2}} \frac{1}{\left[1 + \frac{g_\sigma}{m} \phi(r_j(\theta_j^s))\right]^2} . \quad (38)$$

At this level of the approximation the causality problem with the advanced part of the Green function is not present because the retarded and the advanced fields are identically the same when they are created by charges moving on straight world lines. Therefore one may regard the fields as retarded only. In addition the unsolved problem of radiation reaction, where the radiation acts back on the world lines [15], does not occur because there are no radiation fields any more.

## 2.2 Instantaneous action-at-a-distance

In the spirit of the small acceleration assumption discussed in the previous section one can use the straight line expansion in the action (17) and perform the integration over  $\theta_j$ . This results in an instantaneous action-at-a-distance where the Lorentz-boosted Yukawa fields appear again and there is only one time, the scalar synchronizing time  $t$ ,

$$\mathcal{A} = \int dt \mathcal{L}(r_i(t), u_i(t)) . \quad (39)$$

The Lagrange function is now

$$\mathcal{L}(r_i(t), u_i(t)) = - \sum_{i=1}^A \frac{m_i^*}{u_i^0} \quad (40)$$

$$\begin{aligned} & -\frac{1}{2} \sum_{i,j=1}^A \frac{g_\sigma^2}{4\pi u_i^0} \frac{\exp\left\{-\mu_\sigma \sqrt{R_{ij}^2(t)}\right\}}{\sqrt{R_{ij}^2(t)}} \frac{1}{\left[1 + \frac{g_\sigma}{m} \phi(r_i(t))\right]^2} \frac{1}{\left[1 + \frac{g_\sigma}{m} \phi(r_j(t))\right]^2} \\ & -\frac{1}{2} \sum_{i,j=1}^A \frac{g_\omega^2}{4\pi u_i^0} \frac{\exp\left\{-\mu_\omega \sqrt{R_{ij}^2(t)}\right\}}{\sqrt{R_{ij}^2(t)}} u_{i\alpha}(t) u_j^\alpha(t) \\ & -\frac{1}{2} \sum_{i,j=1}^A \frac{g_\rho^2}{4\pi u_i^0} \frac{\exp\left\{-\mu_\rho \sqrt{R_{ij}^2(t)}\right\}}{\sqrt{R_{ij}^2(t)}} u_{i\alpha}(t) u_j^\alpha(t) \frac{1}{2\tau_i} \frac{1}{2\tau_j} . \end{aligned} \quad (41)$$

The four-positions  $r_i^\alpha(t) \equiv r_i^\alpha(\theta_i(t))$  and 4-velocities  $u_i^\alpha(t) \equiv u_i^\alpha(\theta_i(t))$  are to be taken at the same scalar synchronizing time  $t$  and

$$R_{ij}^2(t) := -(r_i(t) - r_j(t))^2 + \left[ (r_{i\beta}(t) - r_{j\beta}(t)) u_j^\beta(t) \right]^2 \quad (42)$$

The small acceleration approximation together with the introduction of a synchronizing hypersurface  $S(x)$  leads to an equal time lagrangian which is Lorentz-scalar and written in a manifestly covariant way.

Giving up explicit covariance and choosing  $\eta = (1, 0, 0, 0)$  in a special coordinate frame, the positions and velocities take the form

$$r_i(\theta_i(t)) = (t, \vec{r}_i(t)) \quad \text{and} \quad u_i(\theta_i(t)) = \frac{1}{\sqrt{1 - \vec{v}_i^2(t)}} (1, \vec{v}_i(t)) . \quad (43)$$

With that a Lagrange function  $\mathcal{L}(\vec{r}_i(t), \vec{v}_i(t))$  can be defined which depends only on the independent variables and one time.

The advantage of the instantaneous lagrangian is that one can define easily the hamiltonian and the total momentum, which are then strictly conserved by the equations of motion.

### 2.3 Hamilton equations of motion

In the following we want to express the total hamiltonian as a function of the positions  $\vec{r}_i$  and the canonical momenta  $\vec{p}_i$ . Using the Lagrange function given in Eq. (40) the canonical momenta and the energy are determined as

$$\vec{p}_i = \frac{\partial \mathcal{L}}{\partial \vec{v}_i} \quad , \quad (44)$$

$$E = \sum_i \frac{\partial \mathcal{L}}{\partial \vec{v}_i} \vec{v}_i - \mathcal{L} \quad .$$

To be able to perform these derivatives and get an analytical expression for the energy we expand the Lagrange function (40) up to third order in  $(g_\sigma/m)\phi_i$ . Since the  $\phi$  field depends on the nucleon density, this approximation is better at low densities, and its validity should be checked during the calculation. We come back to this point later.

Performing these derivatives the momenta  $\vec{p}_i$  and the energy  $E$  of the system turn out to be

$$\vec{p}_i = M_i \vec{u}_i - \frac{1}{2} \sum_{j \neq i}^A \hat{f}_{ji} u_i^0 \left[ \vec{r}_{ij} (\vec{r}_{ij} \vec{u}_i) + \vec{u}_i (\vec{r}_{ij} \vec{u}_i)^2 \right] N_{ij} + \vec{G}_i , \quad (45)$$

$$E = \sum_{i=1}^A u_i^0 M_i - \frac{1}{2} \sum_{i,j=1}^A \hat{f}_{ji} (\vec{r}_{ij} \vec{u}_i)^2 \left( u_i^0 \right)^2 N_{ij} \quad (46)$$

$$+ \sum_{i=1}^A \frac{(\vec{G}_i \vec{u}_i)}{u_i^0} + \frac{1}{2} \sum_{i,j=1}^A g_{ij} (u_{i\alpha} u_j^\alpha) \frac{1}{u_i^0} ,$$

where

$$M_i = m - \frac{1}{2} \sum_{j \neq i}^A f_{ij} + \frac{1}{m} \sum_{j,k=1}^A f_{ij} f_{jk} \quad (47)$$

$$- \frac{1}{m^2} \sum_{j,k,l=1}^A \left[ 2f_{ij} f_{jk} f_{kl} + \frac{3}{2} f_{ij} f_{jk} f_{jl} - \frac{1}{2} f_{ij} f_{ik} f_{il} \right] ,$$

$$N_{ij} = \frac{1}{u_j^0} - \frac{2}{m} \sum_{k=1}^A \frac{f_{jk}}{u_j^0} - \frac{2}{m} \sum_{k=1}^A \frac{f_{kj}}{u_k^0} + \frac{1}{m^2} \sum_{k,l=1}^A \left[ \frac{2f_{ik} f_{kl}}{u_j^0} + \right. \quad (48)$$

$$\begin{aligned}
& + \frac{2f_{il}f_{kj}}{u_k^0} + \frac{3f_{kj}f_{jl}}{u_k^0} - \frac{3f_{jk}f_{jl}}{2u_j^0} \Big] \\
\vec{G}_i &= \frac{1}{2} \sum_{j \neq i}^A \left( g_{ij} + \frac{u_i^0}{u_j^0} g_{ji} \right) \vec{u}_j - \frac{1}{2} \sum_{j \neq i}^A g_{ji} \left[ \left( u_i^0 \right)^2 - \frac{u_i^0}{u_j^0} \vec{u}_i \vec{u}_j \right] \vec{u}_i \\
& + \frac{1}{2} \sum_{j \neq i}^A \hat{g}_{ji} \left[ \left( u_i^0 \right)^2 - \frac{u_i^0}{u_j^0} \vec{u}_i \vec{u}_j \right] \left[ \vec{r}_{ij} (\vec{r}_{ij} \vec{u}_i) + \vec{u}_i (\vec{r}_{ij} \vec{u}_i)^2 \right] .
\end{aligned} \tag{49}$$

In these expressions  $f_{ij}$  and  $g_{ij}$  are

$$\begin{aligned}
f_{ij} &\equiv f(R_{ij}) = \frac{g_\sigma^2}{4\pi} \frac{\exp\{-\mu_\sigma R_{ij}\}}{R_{ij}} , \quad R_{ij}^2 = \vec{r}_{ij}^2 + (\vec{r}_{ij} \vec{u}_j)^2 , \quad \vec{r}_{ij} = \vec{r}_i - \vec{r}_j , \\
g_{ij} &= \frac{g_\omega^2}{4\pi} \frac{\exp\{-\mu_\omega R_{ij}\}}{R_{ij}} + \frac{g_\varrho^2}{4\pi} \frac{\exp\{-\mu_\varrho R_{ij}\}}{R_{ij}} \frac{1}{2} \tau_i \frac{1}{2} \tau_j , \\
\hat{f}_{ji} &\equiv -\frac{1}{R_{ji}} \frac{d}{dR_{ji}} f(R_{ji}) = \frac{g_\sigma^2}{4\pi} (1 + \mu_\sigma R_{ji}) \frac{\exp\{-\mu_\sigma R_{ji}\}}{R_{ji}^3} ,
\end{aligned} \tag{50}$$

and  $\hat{g}_{ji}$  is defined in the same way as  $\hat{f}_{ji}$ . It is worthwhile to note that  $f_{ij} \neq f_{ji}$ .

Let us first prove that for homogeneous and isotropic nuclear matter, like in the original mean-field picture [16] the vector potential will not contribute to the canonical momentum. In that case the summation can be replaced by an integration over space and momentum, folded with the phase space distribution function. Since for homogeneous nuclear matter the distribution function is independent of the position, the space integral can be carried out immediately and the remaining part is written as a summation over momenta. Finally for infinite nuclear matter we get

$$\begin{aligned}
\vec{p}_i &= m^* \vec{u}_i , \quad m^* = m - B + \frac{3B^2}{m} - 12 \frac{B^3}{m^2} , \quad B = \left( \frac{g_\sigma}{\mu_\sigma} \right)^2 \frac{1}{\Omega} \sum_i \frac{1}{u_i^0} \\
E_{nm} &= \sum_i \left[ m^* u_i^0 + \frac{1}{2u_i^0} \left( B - 4 \frac{B^2}{m} + 18 \frac{B^3}{m^2} \right) + \frac{1}{2} \left( \frac{g_\omega}{\mu_\omega} \right)^2 (j^0) \right] .
\end{aligned} \tag{51}$$

Expression (52) is exactly the one in Ref. [8] for low density expansion.

It is worthwhile to mention that the small acceleration approximation which introduces  $R_{ij}$  instead of  $|\vec{r}_{ij}|$  in Eq. (50), is definitely needed to get back the relativistic mean-field result for nuclear matter. Hence we take for the strengths  $g_\sigma$  and  $g_\omega$  the values obtained from the saturation properties of the nuclear matter [13].

To be able to apply the above method for QMD calculation we have to get

the energy as a function of  $\vec{p}_i$  and  $\vec{r}_i$ . In order to get this we use Eq. (45) to express  $\vec{u}_i$  as a function of the momentum  $\vec{p}_i$  by expanding up to third order in  $f_{ij}/m$ ,  $g_{ij}/m$  and  $\vec{p}_i^2/m^2$ . After substituting  $\vec{u}_i$  into Eq. (46) the energy is

$$\frac{E}{mc^2} = \underbrace{\sum_i \sqrt{1 + \vec{p}_i^2}}_{E_{kin}} - \frac{1}{2} \sum_{i,j=1}^A \underbrace{\frac{\tilde{f}_{ij}}{\sqrt{1 + \vec{p}_i^2} \left( 1 + 2 \sum_{k=1}^A f_{jk} \right)}}_{E_S} + \frac{1}{2} \sum_{i,j=1}^A \underbrace{\tilde{g}_{ji} \sqrt{1 + \vec{p}_i^2}}_{E_V} - \frac{1}{2} \sum_{i,j=1}^A \underbrace{\tilde{g}_{ji} \frac{(\vec{p}_i \vec{p}_j)}{\sqrt{1 + \vec{p}_i^2}}}_{E_{p_i p_j}} + \underbrace{\frac{1}{2} \sum_i \left( \sum_{i,j=1}^A \tilde{f}_{ji} \vec{p}_i - \sum_{i,j=1}^A \tilde{g}_{ji} \vec{p}_j \right)^2 + \sum_{i,j,k,l=1}^A \left( \tilde{f}_{ij} \tilde{f}_{jk} \tilde{f}_{kl} - \tilde{f}_{ij} \tilde{f}_{ik} \tilde{f}_{il} - \tilde{f}_{ij} \tilde{f}_{jk} \tilde{f}_{kl} \right)}_{E_3} \quad (52)$$

where  $\tilde{f}_{ij}$  and  $\tilde{g}_{ij}$  are now functions of

$$R_{ij}^2 = \vec{r}_{ij}^2 + (\vec{r}_{ij} \vec{p}_j)^2 \quad , \quad (53)$$

with  $\vec{p}_i = \vec{p}_i/mc$ ,  $\tilde{f}_{ij} = f_{ij}/mc^2$ ,  $\tilde{g}_{ij} = g_{ij}/mc^2$ .  $E_{kin}$ ,  $E_S$ ,  $E_V$ ,  $E_{p_i p_j}$  denote the kinetic, scalar, vector term, respectively and  $E_3$  is of third order and hence small, as we show later.

From Eq. (52) the Hamilton equations

$$\frac{d}{dt} \vec{r}_i = \frac{\partial E}{\partial \vec{p}_i} \quad \frac{d}{dt} \vec{p}_i = - \frac{\partial E}{\partial \vec{r}_i} \quad (54)$$

are calculated easily.

### 3 Details of the QMD calculations

Quantum Molecular Dynamics is a classical many-body theory in which some quantum features due to the fermionic nature of nucleons are simulated. For the details of the theory we would like to refer the reader to the works of Aichelin [5] and the Frankfurt group [6].

### 3.1 The initial conditions

Although in our calculations up to now we considered the nucleons as point particles, to determine the initial space and momentum distribution of the ground-state nuclei in their own rest frame we used the same procedure as described in Ref. [5] and [17,18]. The nucleons were characterized both in coordinate and momentum space with gaussians, with the Wigner density

$$f_{n,p}(\vec{r}, \vec{p}, t) = \frac{1}{(\pi\hbar)^3} \sum_i e^{-\alpha^2|\vec{r}-\vec{r}_i(t)|^2} e^{-\beta^2|\vec{p}-\vec{p}_i(t)|^2}. \quad (55)$$

The width  $\alpha$  was chosen such that placing the nucleons on a lattice for infinite nuclear matter calculation we get a smooth distribution with proper binding energy and saturation density. Since the scalar and vector interactions of the lagrangian describe the long-range part of the nucleon-nucleon interaction, the mean-field, whereas the short range repulsion is treated explicitely by the collision term, a cutoff has to be introduced at short distances to separate both. This is done by folding the Yukawa functions  $f_{ij} = f(R_{ij})$  with the gaussian density distribution introduced in Eq. (55) for the phase-space density [2]. Due to the folding the forces depend on the width parameter  $\alpha$ . A proper choice should give a reasonably smooth mean field at nuclear matter density and at the same time be in accord with the cross section which determines the distance of closest approach below which random scattering occurs. We found, that the best value of  $\alpha$ , satisfying the above requirements was  $\alpha \approx 0.55\text{fm}^{-1}$ . Choosing for example  $\alpha = 0.7\text{fm}^{-1}$ , we could not get a satisfactorily smooth distribution for nuclear matter on the lattice. The parameter  $\beta$  in (55) was determined as  $\beta = 1/(\hbar\alpha)$ .

We construct the ground state of the gold nucleus by distributing the centers of the Gaussians so that the resulting configurations yield a binding energy per nucleon within 0.1 MeV of the experimental value of 7.9 MeV, and  $|\vec{r}_i - \vec{r}_j| |\vec{p}_i - \vec{p}_j| > d$ , where  $d$  is in the order of  $\hbar$ . The initialization of the colliding system is performed by boosting two such nuclei relativistically towards each other, so that in the center of momentum frame two Lorentz contracted nuclei are colliding.

### 3.2 The mean-field forces

The ZM forces derived in the previous section give saturation without the introduction of a nonlinear scalar potential, originally proposed by Boguta [7], and used in many mean-field calculations. This way we have less free parameters, than usual. Furthermore fixing the masses of the scalar and vector

	$g_\sigma$	$g_\omega$	$g_\rho$	$\mu_\sigma c^2$	$\mu_\omega c^2 = \mu_\rho c^2$	$m^*$	$\kappa$	$\varrho_0$
W	11.04	13.74	7.0	550	783	0.54	550.8	0.148
ZM	7.84	6.67	7.0	550	783	0.85	224.7	0.160
used	7.22	5.58	7.0	550	783	0.8	212.1	0.158

Table 1

Parameters of the Walecka Zimányi-Moszkowski and our forces. The meson masses are given in MeV/c<sup>2</sup>, the compressibility in units of MeV and the densities are in fm<sup>-3</sup>.

mesons to their generally accepted values the only remaining free parameters are the meson coupling constants,  $g_\sigma$ ,  $g_\omega$  and  $g_\rho$ , which are determined from the ground state properties of nuclear matter and the symmetry energy. We summarize the parameters used in this work and the resulting properties of the ZM force together with those of Walecka lagrangian in Table 1. As one can see, the ZM force needs much smaller values of the coupling constants, and yields also a much smaller compression coefficient. In our calculation we are using the expanded form (52) of the exact energy expression (46), and in order to keep the nuclear matter parameters, we modified the ZM parameters accordingly. The values of the parameters for different forces are summarized in Table 1. The Coulomb energy although not explicitly mentioned, is included as a zero mass vector interaction.

We would like to emphasize, that no additional momentum dependent forces are introduced, the momentum dependence is a generic property of the relativistic force and cannot be changed. It is therefore interesting to compare the predicted value of observables, which depend strongly on the momentum dependence, like different flow values, with the measured ones.

### 3.3 The treatment of the collision term

For the cross section in the collision term we used the Cugnon one [19] and for the Pauli blocking the same method as is described in Ref [2,17]. The individual two-body collision is calculated in a relativistically covariant way, as given in [20], the only difference is that instead of the bare mass of the nucleons,  $m$ , we use the effective mass,  $m^*$ , as explained below.

In an interacting many-body system single-particle energies  $e_i$  cannot be defined such that  $(e_i, \vec{p}_i)$  form a 4-vector. Only the total momentum  $\vec{P}$  and total energy  $E$  combine to a 4-vector. However, we still try to deduce a single particle energy, which we use for the conservation of energy in each binary collision.

Equation (52) in leading order in  $\vec{\tilde{p}}_i$  and  $\tilde{f}_i, \tilde{g}_i$  can be written as

$$\frac{E}{mc^2} = \sum_{i=1}^A \sqrt{1+\vec{\tilde{p}}_i^2} - \frac{1}{2} \sum_{\substack{i,j=1 \\ j \neq i}}^A \frac{\tilde{f}_{ij}}{1+2\sum_{\substack{k \\ k \neq j}} \tilde{f}_{jk}} \frac{1}{\sqrt{1+\vec{\tilde{p}}_i^2}} + \frac{1}{2} \sum_{\substack{ij=1 \\ j \neq i}}^A \tilde{g}_{ji} \sqrt{1+\vec{\tilde{p}}_i^2} \quad (56)$$

There are two ways to define the effective mass  $m_i^*$  appearing in the collisions:

Case A: If we neglect the momentum dependence in  $\tilde{f}_{ij}$  and  $\tilde{g}_{ij}$ , the energy of the  $i^{\text{th}}$  particle can be written as

$$\begin{aligned} \frac{\epsilon_i}{mc^2} &= \frac{E(A) - E_i(A-1)}{mc^2} = \sqrt{1+\vec{\tilde{p}}_i^2} - \frac{1}{2} \sum_{\substack{j \\ j \neq i}} \frac{\tilde{f}_{ij}}{\sqrt{1+\vec{\tilde{p}}_i^2}} \frac{1}{1+2\sum_{\substack{k \\ k \neq j}} \tilde{f}_{jk}} \\ &\quad + \frac{1}{2} \sum_{\substack{j \\ j \neq i}} \tilde{g}_{ji} \sqrt{1+\vec{\tilde{p}}_i^2} + \text{terms independent of } \vec{\tilde{p}}_i, \end{aligned} \quad (57)$$

where  $E_i(A-1)$  means the energy of the system when particle  $i$  is taken out.

We can expand Eq. (57) in  $\vec{\tilde{p}}_i^2$  and get

$$\frac{\epsilon_i}{mc^2} = \frac{1}{2} \vec{\tilde{p}}_i^2 \left[ 1 + \frac{1}{2} \sum_{\substack{j \\ j \neq i}} \frac{\tilde{f}_{ij}}{1+2\sum_{\substack{k \\ k \neq j}} \tilde{f}_{jk}} + \frac{1}{2} \sum_{\substack{j \\ j \neq i}} \tilde{g}_{ji} \right] + \epsilon_{i0}.$$

This can be written as

$$\frac{\epsilon_i}{mc^2} = \sqrt{\left(\frac{m_i^*}{m}\right)^2 + \vec{\tilde{p}}_i^2} + \epsilon'_{i0},$$

where the effective mass  $m_i^*$  turns out to be

$$\frac{m_i^*}{m} = 1 - \frac{1}{2} \sum_{\substack{j \\ j \neq i}} \frac{\tilde{f}_{ij}}{1+2\sum_{\substack{k \\ k \neq j}} \tilde{f}_{jk}} - \frac{1}{2} \sum_{\substack{j \\ j \neq i}} \tilde{g}_{ji}, \quad (58)$$

while  $\epsilon_{i0}$  and  $\epsilon'_{i0}$  are quantities independent of  $\vec{\tilde{p}}_i$ .

Case B: If we assume, that the momentum dependence of  $\tilde{f}_{ij}$  and  $\tilde{g}_{ji}$  is the

same as in nuclear matter, that is

$$E = \sum_i \sqrt{1 + \vec{p}_i^2} - \frac{1}{2} \sum_{\substack{i,j \\ j \neq i}} \frac{\tilde{f}(r_{ij})}{\sqrt{1 + \vec{p}_i^2} \sqrt{1 + \vec{p}_j^2}} \frac{1}{1 + 2 \sum_{\substack{k \\ k \neq i}} \tilde{f}(r_{jk})} + \frac{1}{2} \sum_{\substack{i,j \\ j \neq i}} \tilde{g}(r_{ji}), \quad (59)$$

and the effective mass for finite systems turns out to be

$$\frac{m_i^*}{m} = 1 - \sum_{\substack{j \\ j \neq i}} \frac{\tilde{f}(R_{ij})}{1 + 2 \sum_{\substack{k \\ k \neq j}} \tilde{f}(R_{jk})}. \quad (60)$$

We found in the calculations that the two definitions give nearly the same results. Since Eq. (58) gave slightly better energy conservation, that is what we used.

#### 4 Comparison with experimental data

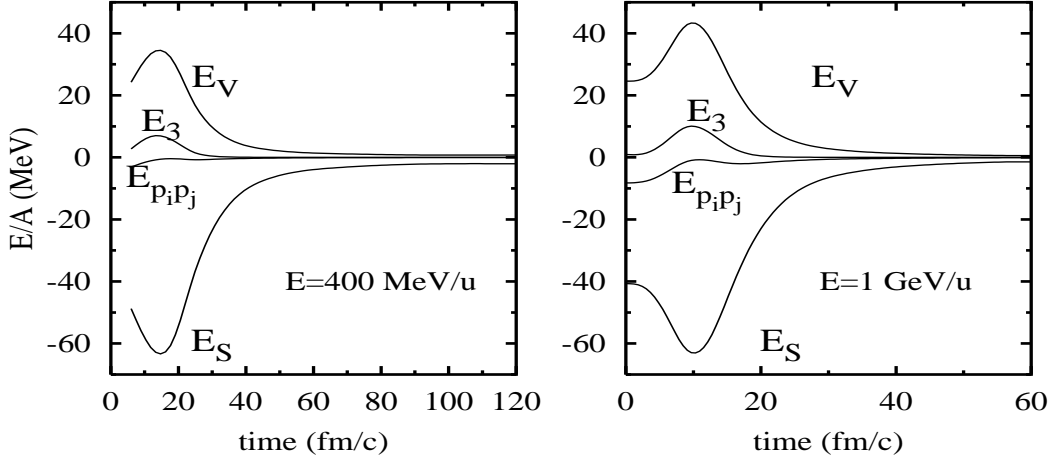


Fig. 2. Time evolution of the average scalar ( $E_S$ ) and vector ( $E_V$ ) energy and the third order ( $E_3$ ) and momentum dependent ( $E_{p_i p_j}$ ) terms at 400 AMeV (left) and 1 AGeV (right). (See Eq. (52).)

We want to apply the relativistically invariant force in the regime of 0.5–2 AGeV bombarding energy. However, the influence of particle creation may blur the effects of the relativistic mean-field forces. For this reason we investigate the features of such a force at lower bombarding energies (150–400 AMeV) and compare our results with the available experimental data. As a first step, we should check the approximation (52) obtained by expressing the four-velocities as functions of the momenta. In Fig. 2 the time evolution of the different energy

terms appearing in Eq. (52) are given as the function of time. One can see that the third order term is small and the approximation is very good for 400 AMeV and is still acceptable even for 1 AGeV.

In presenting our theoretical results, we generally show two kinds of quantities: filtered and unfiltered values. The unfiltered value is the result of the calculation. The filtered values are the results obtained after using the experimental filter due to the experimental hardware (reduction in the  $4\pi$  geometry, detection of low energy particles, etc.). Furthermore, in both case we may apply cuts (event selection criteria), or present the data without these cuts.

Since we wish to compare our results with the FOPI experiments, where the most central collisions were investigated, as a first step, we examine the connection between the experimental centrality condition and the impact parameter in our model.

In Ref. [1] it was decided that centrality depends on the so-called ERAT values and the directivities. These quantities were defined as

$$\text{ERAT} = \frac{\sum_i p_{ti}^2 / (m_i + E_i)}{\sum_i p_{li}^2 / (m_i + E_i)} \quad , \quad D = \frac{|\sum_i Z_i \vec{u}_{ti}|}{\sum_i Z_i |\vec{u}_{ti}|} . \quad (61)$$

The measured protons and nuclei have rest mass  $m_i$ , charge  $Z_i$ , longitudinal momentum  $p_{li}$  and transverse momentum  $p_{ti}$ . The relation to the energy  $E_i$  and the 4-velocity  $u_i$  is as usual. The sum is calculated for all *charged* fragments. The (experimental) selection of the events to get 200 mb total cross section (ERAT200) for 400 AMeV gold-gold collisions corresponds to  $\text{ERAT} > 0.66$ , the 50 mb value (ERAT50) corresponds to  $\text{ERAT} > 0.88$ . Experimentally, these cuts were still not found satisfactory for selecting central events, and an additional directivity cut was applied for the ERAT200 set with  $D < 0.19$  defining the ERAT200D set. The directivity is defined in Eq. (61).

$b$ (fm)	ERAT200		ERAT200D		ERAT50	
	400	150	400	150	400	150
0.5	98	67	84	63	72	15
1.0	95	64	48	51	36	14
1.5	95	38	34	28	37	5
2.0	82	18	21	8	6	2
2.5	59	10	5	5	3	-
3.0	27	8	3	4	-	-

Table 2

Acceptance of the QMD events in percentage in the case of different cuts for several impact parameters at 400 and 150 AMeV.

In our comparison we mostly use a cut in the impact parameter. To see how reliable this is, we compare our total ERAT distributions for different energies

with the experimental ones. As one can see in Fig. 3, for 150 AMeV the agreement is excellent, and it is still satisfactory for higher energies.

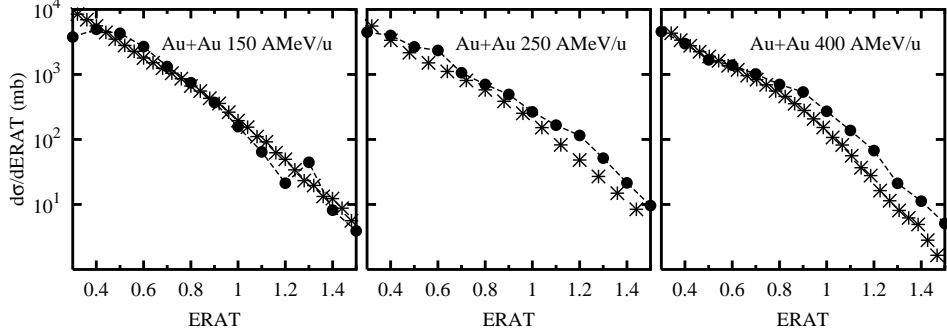


Fig. 3. Measured ERAT distribution (crosses) [1] at 150 AMeV (left), 250 AMeV (middle) and 400 AMeV (right) and results of QMD calculations with the experimental filter (solid line with dots).

As a next step, we calculate the percentage of the accepted events for different cuts as the function of the impact parameter. In Table 2 we show the correlation between the impact parameter and various experimental cuts. One can see, that the cut ERAD200D, used mostly in the evaluation of the experimental data, gives good centrality. In our calculation we choose the centrality according to the impact parameter. However, to determine the importance of the ERAT cuts, we sometimes follow the original recipe selecting events according to their ERAT values, and compare the results of the two selection methods. If we average over impact parameters up to  $b = 2$  fm, the values are very similar to the ones obtained with the selection ERAT200D.

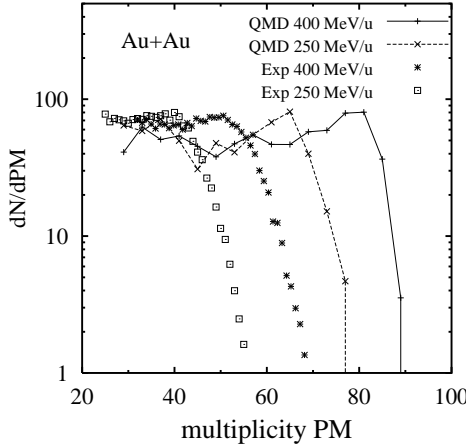


Fig. 4. Measured and calculated multiplicity distribution at two beam energies.

Before comparing the theoretical results with the experimental ones, we should mention a common shortcoming of all the QMD calculations. Since shell effects are absent the number of protons is overestimated and the abundance of alpha particles ( $Z = 2$ ) underestimated. Therefore the total multiplicity is larger

than the experimental one (see Fig. 4). The same phenomena can be observed in the rapidity distributions. At 400 AMeV the distributions of the heavier fragments are more or less agreeing with the experimental values, however, for  $Z = 1$  and  $Z = 2$ , while the calculated shapes are good, the absolute values are not. If the calculated  $Z = 1$  distribution is scaled by a factor  $2/3$  down to the measured one and the remaining  $1/3$  of the protons is appointed to the  $Z = 2$  distribution a consistent picture is achieved, as is shown in Fig. 5.

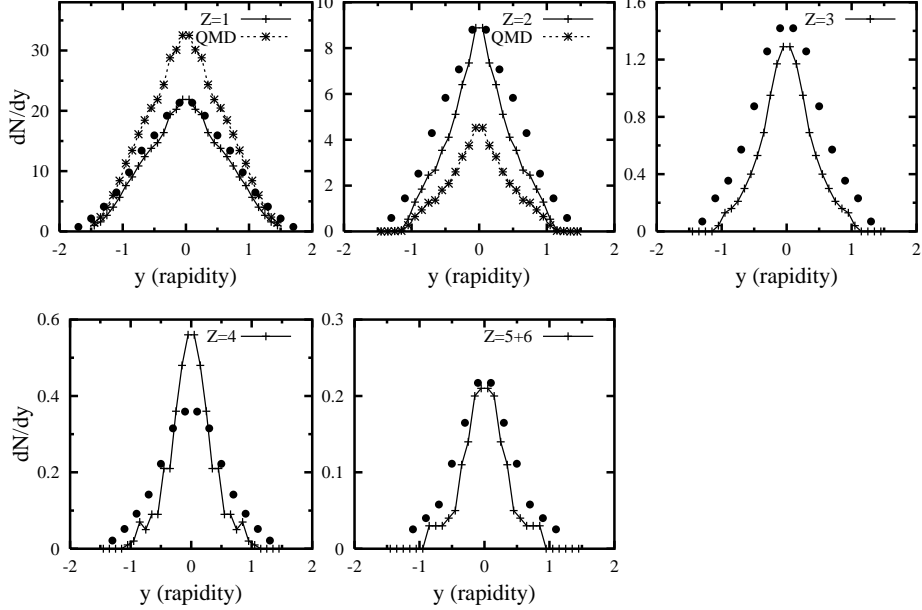


Fig. 5. Measured rapidity distributions (dots) [1] at 400 AMeV for various nuclear charges. The solid line with crosses is the result of the model calculation, while the dashed lines for  $Z = 1$  and  $2$  with crosses correspond to the scaled model calculation (see text).

The measured ( $4\pi$  averaged) charge distributions also agree well with the calculated ones. The tail of the distribution obtained with an impact parameter cut  $b \leq 1.5\text{fm}$  in the calculations at 150 AMeV slightly differs from the experimental one, however, when applying the ERAT200D cut on the calculated events, the overestimation for large charge numbers disappear (see Fig. 6). This means that the ERAT200D cut throws out those central events which have bigger fragments. For higher energies the none of the ERAT cuts modify the picture significantly which is in accord with the experimental findings [1].

One important quantity which is characteristic of multifragmentation is the number of intermediate mass fragments (IMF,  $2 < Z < 30$ ). The number of IMFs is a crucial test for the capability of the model to describe many-body correlations. There is however the complication that the fragments are altered by subsequent decay before they reach the counter. The modification of the distributions will be stronger if the fragments are created with high excitation

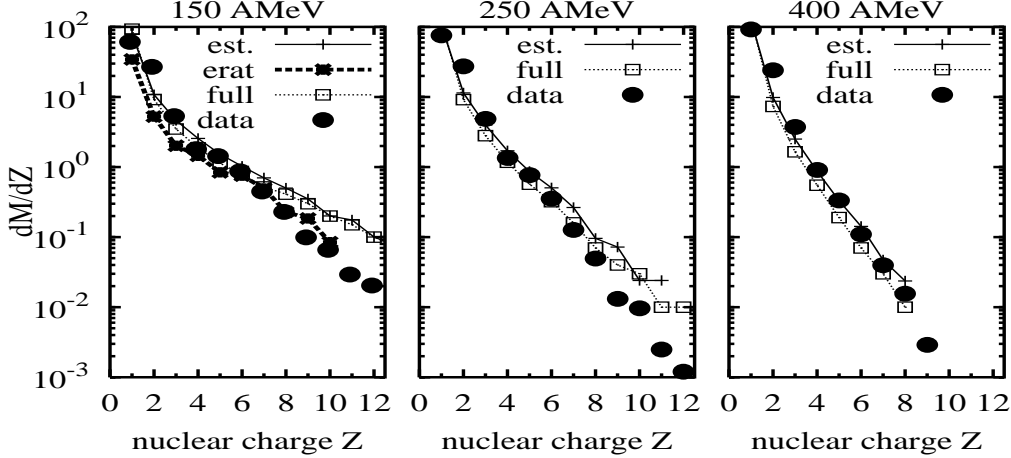


Fig. 6. Measured (dots) and calculated charge distributions at three incident energies. The solid line with crosses corresponds to filtered QMD events for  $b \leq 1.5\text{fm}$  extrapolated to  $4\pi$  geometry (est.), while the dashed line with squares is the QMD unfiltered calculation for  $b \leq 1.5\text{fm}$ . For 150 AMeV the calculation performed with ERAT200D cut (thick dashed line with crosses) is also presented.

energy. At the end of our QMD calculation the fragments are bound, with an excitation energy of 1–2 MeV per particle. At these energies deexcitation occurs mainly through radiation and sometimes by particle emission, therefore the final mass numbers of the fragments will change only slightly. In Fig. 7, we show the filtered and unfiltered IMF distributions as the function of the impact parameter for the different energies. Contrary to most theoretical calculations, which substantially underestimate the IMF distribution in central collisions, our model yields values much closer to the measured ones. We also studied how the number of IMFs depend on the assumption or approximations made in the model.

To determine the effect of the effective mass on multifragmentation, we used for  $m^*$  both of the expressions (58) and (60) and in addition we also performed calculations with  $m^*$  set to  $m$  [22] in the collision term.

The choice of the effective mass influenced the number of IMF values less than 6%. The choice  $m^* = m$  in the collision term always yielded the largest  $\langle M_{IMF} \rangle$ . Neglecting the third order term in Eq. (52), but readjusting the coupling strengths such that the saturation density was kept at its correct value, the change was less than 3%, thus completely negligible. A 20% change in the collision cross section also gave less than 7% change.

In addition we calculated the azimuthal distribution of the IMFs at 250 AMeV, and found a good agreement with the experimental values. In Fig. 8 the experimental data [1] are compared to

$$dM/d\phi = a_0(1 + a_1 \cos \phi + a_2 \cos 2\phi) \quad (62)$$

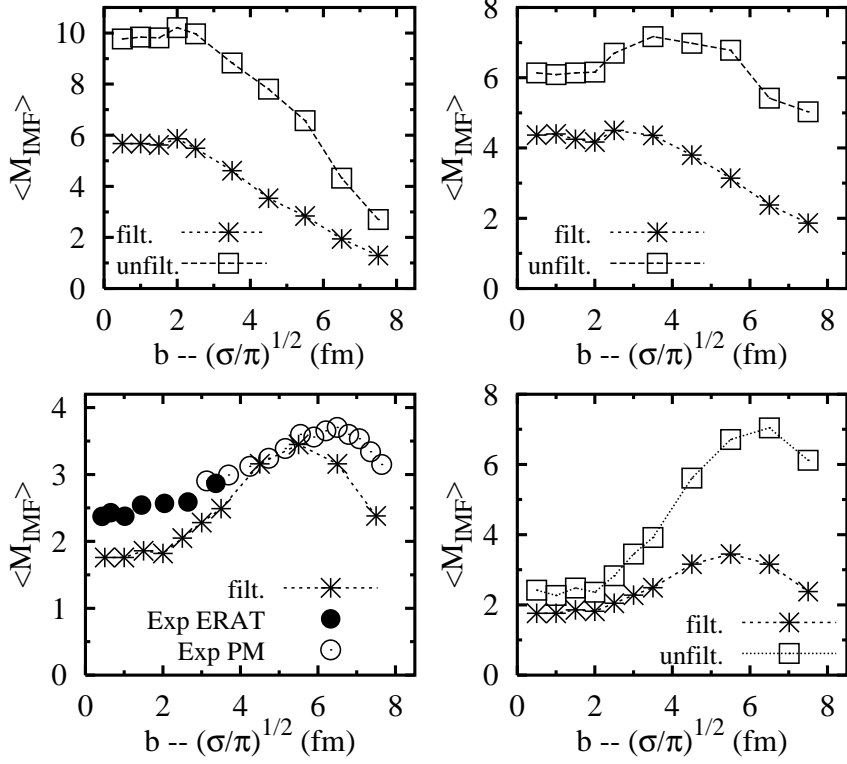


Fig. 7. Number of IMF-s as a function of impact parameter at three incident energies (150 AMeV – upper left, 250 AMeV – upper right and 400 AMeV – lower line) with and without filtering the QMD calculation, and the experimental values at 400 AMeV [1].

which was fitted to the calculated numbers. The ratio  $R = \frac{dM/d\phi(\phi=0)}{dM/d\phi(\phi=\pi)}$  is also indicated.

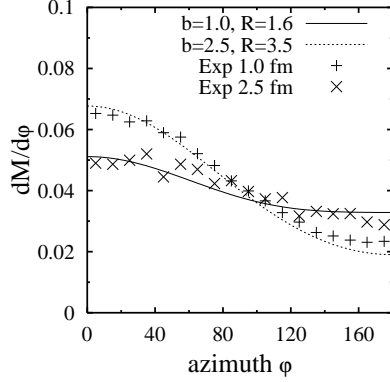


Fig. 8. Azimuthal angle distribution of intermediate mass fragments using the ERAT filter for 250 AMeV. Dots represent the experimental data [1], while the solid lines are fits (62) to the QMD calculations.

In Figs. 10 and 9 the scaled transverse four-velocity distribution  $dM/u_t du_t$  is shown for forward particles (with  $y > 0.5$ ) and for particles around midrapidity ( $y < 0.5$ ). The lines are taken from the experimental data [1], while the dots

and squares represent the results of the QMD calculations for central collisions in the impact parameter range  $0 < b \leq 2.5\text{fm}$  and the ERAT200D cut. For  $Z = 1$  and  $E = 150\text{AMeV}$  the ERAT200D cut has little influence. Both calculated spectra agree with the data. For  $Z = 2$  the situation is different, the ERAT200D cut seems to select events which have about 5 times more  $\alpha$  particles.

Fig 9 shows agreement in the spectra for  $E = 400\text{AMeV}$  and  $Z = 1$  while the calculated  $Z = 2$  spectra deviate substantially. Here the ERAT200D selection has little influence on the spectra in contrast to the  $E = 150\text{AMeV}$  displayed in Fig. 10. For 400 AMeV energy there is no deviation between the ERAT cut and the impact parameter cut.

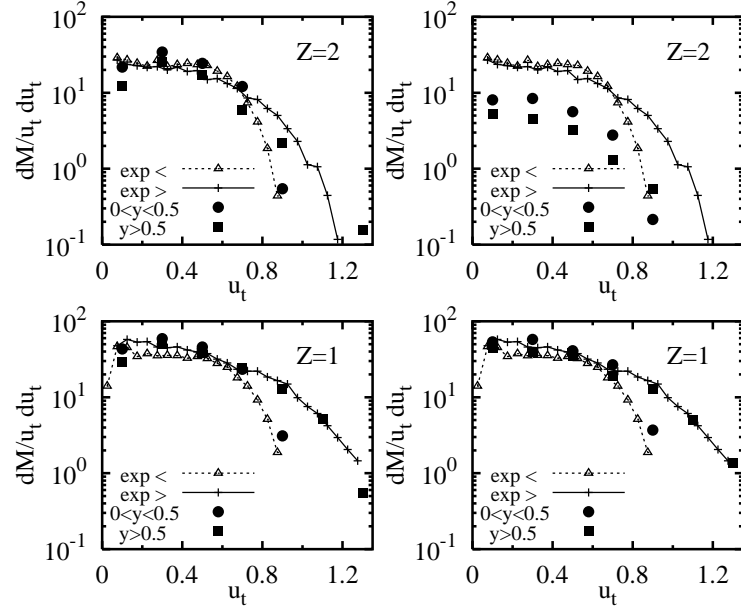


Fig. 9. Invariant transverse four-velocity spectra at 150 AMeV with ERAT200D cuts (left block) and at  $0 < b \leq 2.5\text{fm}$  (right block) for protons and alpha particles.

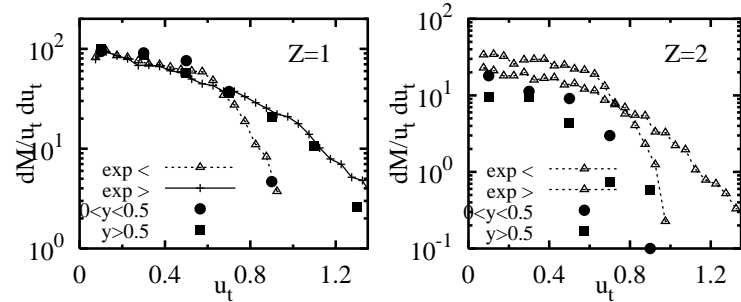


Fig. 10. Invariant transverse four-velocity spectra at 400 AMeV and  $0 < b \leq 2\text{fm}$  for  $Z = 1$  and  $2$ .

## 5 Collective flow and the kinetic energies of large fragments

Due to its sensitivity, flow is one of the most important data provided by the experiments to test the theoretical models. One can distinguish three types of flow: the side, the squeeze-out and the spherical. The first two are well known, and have been studied extensively both experimentally [23] and theoretically [24] for a long time. We present the integrated side flow,

$$p_x^{\text{dir}} = \sum_i Z_i u_{xi} / \sum_i Z_i, \quad (63)$$

in Fig. 11a as the function of the impact parameter. The agreement with the experimental values is remarkable.

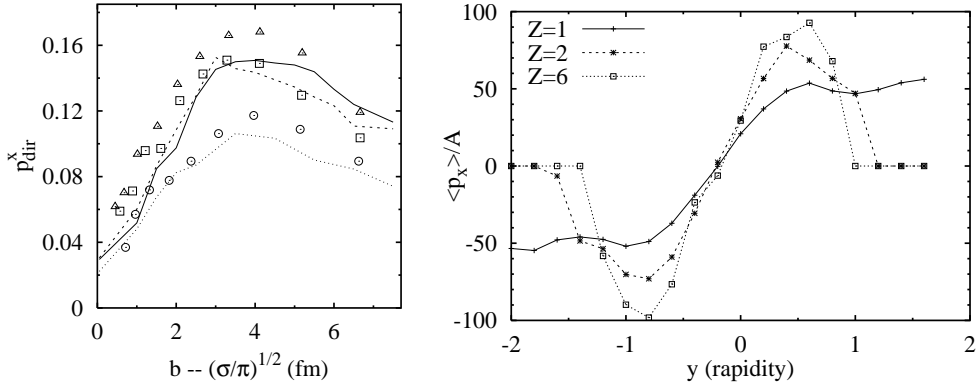


Fig. 11. **a** Measured (symbols) and calculated (lines) integrated scaled side flow as the function of the impact parameter at an incident energy of 150 (triangle and solid line), 250 (square and dashed line) and 400 AMeV (circle and dotted line) (left). **b** Side flow for various nuclear charges at an incident energy of 400 AMeV as the function of the rapidity (right).

In Fig. 11b we present the side flow for different fragment masses as the function of the rapidity at bombarding energy of 400 AMeV. The side flow increases with the increase of the fragment mass, which is in accordance with the experimental observation [23].

Recently interest has been focused on a third type of flow both experimentally [1] and theoretically [25], namely the so called central (or radial) flow, which is most prominent in central collisions where the side flow already disappears. Experimentally, it was found, that the kinetic energy of the fragments increases as their mass number increases. Although our calculation does not reproduce the experimental amount of the kinetic energy, we also obtained a curve which shows a significant increase (see Fig. 12).

The reason for the difference between the theoretical and experimental values

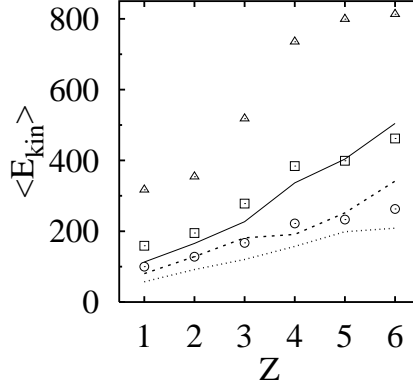


Fig. 12. Measured (symbols) and calculated (lines) average kinetic energy as the function of the fragment charge number for 150 (circles and dotted line), 250 (squares and dashed line) and 400 AMeV (triangles and solid line), summed up to  $b = 2.5 \text{ fm}$  impact parameters.

is the following: on examining the structure of the  $A > 6$  fragments, it can be observed that they are sometimes a mixture of target and projectile nucleons. Since this means that the nucleons in the fragments collided many times, at the freeze-out density they are still not too far from the center, hence their kinetic energy is small. It also can occur that the fragments consist almost completely of either target, or projectile nucleons, which move together during the collision and only rarely interact with other nucleons. In this case the kinetic energy of the fragment is large. However, these fragments move mainly in a forward direction, so their ERAT value is smaller than the experimental cut will allow. In Fig. 13a we give the fragments' average distance from the center as the function of their mass, where the above-mentioned tendency is clearly seen. For large impact parameters, the large and small fragments move together.

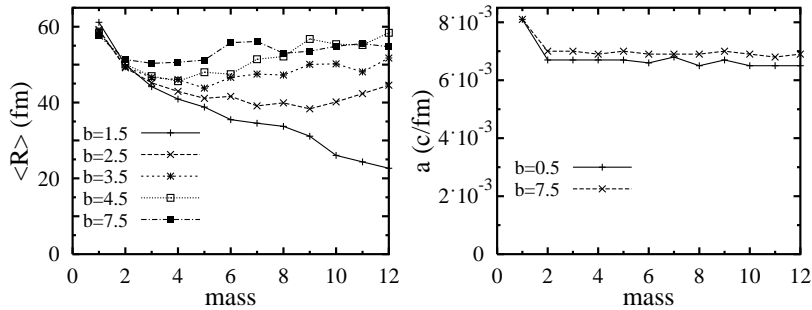


Fig. 13. **a.** Average distance of the fragments (in fm) from the center of mass as the function of their mass at 400 AMeV (left). **b.** The radial velocity parameter,  $a^{(M)}$ , as the function of the fragment mass at 400 AMeV (right). Both curves were calculated at  $t = 150 \text{ fm/c}$ .

If we determine the velocity of the fragment from an assumed blast profile,

Table 3

Flow energies (MeV), “thermal” energies and average flow velocities ( $\beta$ ) at 400 (upper), 250 (middle) and 150 AMeV (lower part) at an impact parameter of  $b=1$  fm.

A MeV	$E_{\text{flow}}$	$E_{\text{flow}}^{\text{exp}}$	$E_{\text{th}}$	$E_{\text{th}}^{\text{exp}}$	$\beta$	$\beta^{\text{exp}}$
400	59.7	57.8	32.7	32.8	0.338	0.334
250	34.8	34.0	16.8	21.5	0.264	0.263
150	18.3	19.9	10.2	12.6	0.194	0.204

$$\vec{u}_i = a \vec{r}_i \quad , \quad a^{(M)} = \frac{\sum_i \vec{u}_i \vec{r}_i}{\sum_i r_i^2} \quad (64)$$

and perform the summation only for clusters with mass  $M$ , we can also obtain the  $a$  value as the function of the mass. Fig. 13b show, that  $a$  is almost independent of the mass.

Experimentally, the central flow energy is evaluated with the help of the blast model from the mass number dependence of the measured kinetic energies. In this method, the contribution of the small number of the larger fragments dominates the final result. Since in our case the kinetic energies of the big fragments are not large enough, we had to apply a different method to determine the central flow.

Considering that the total mass of the large fragments together is small compared to the total mass of the two colliding nuclei, we decided to determine the central flow and flow energy using all the particles [26]. We divided the total solid angle into 32 parts and calculated the average velocity, as much as the number of particles in each section. The fluctuation of the averages was less than 2% and 4%, respectively at 400 AMeV for central events ( $b \leq 1\text{ fm}$ ).

Our conclusion was that up to an impact parameter of 2 fm there is a significant central flow, and the concept of thermal energy, which is based on the thermalization, can be used. The values calculated from our model agree with the ones which were obtained from the experiments using the blast model (see Table 3 and for the details Ref. [26]).

## 6 Freeze-out

An important concept for understanding the dynamics of multifragmentation is the occurrence of freeze-out. After the violent initial phase of the collision with a rapid increase of entropy, density and local excitation energy the system begins to expand and cool. Freeze out characterizes the situation where the particles are far enough from each other so that they are not colliding any more. If this happens throughout space in a narrow time interval one may define a freeze-out time.

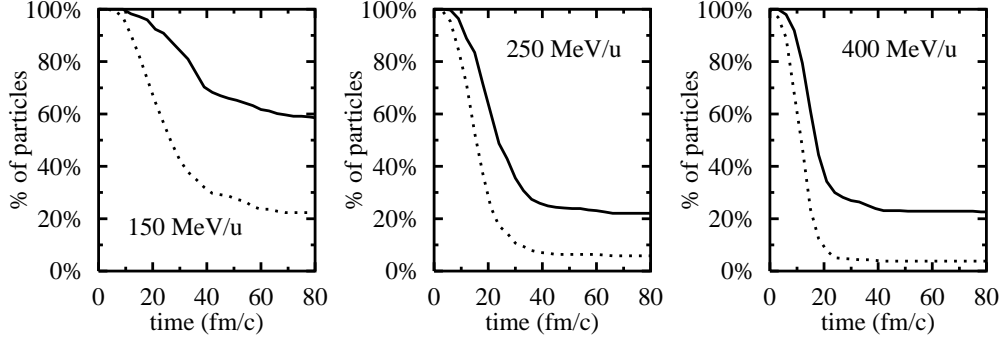


Fig. 14. Number of particles which collided less than three times (solid line), and which did not collide at all (dotted line) for three incident energies, at an impact parameter of  $b = 0.5 fm$ , as the function of time.

Depending on the speed of the expansion freeze-out will “freeze” the mass distribution and the velocity of the nucleons and cluster in different situations on the way towards equilibration. One way of recognizing that freeze-out is happening is to observe that the number of unblocked collisions are drastically decreasing. It is clear that some collision can still occur even after freeze out, because some of the nucleons which lost their energy and are still near the center (about 5% of all nucleons) are nevertheless close enough to each other to be able to collide. The nucleons within the clusters can also collide with each other, however, the number of such collisions is small. In Fig. 14, we show as the function of time the fraction of nucleons which did not collide at all and those that collided less than three times. For 400 AMeV and 200 AMeV one observes that already after 30 fm/c the fraction of particles which did not suffer a collision does not decrease anymore because they have escaped. The same holds true for those which collide three or more times (percentage above full line) so that one can assume that after 30 fm/c no further equilibration takes place.

In Fig. 15, the number of collisions is displayed as the function of time for 150, 250 and 400 MeV. Also From these results it can be seen, that freeze-out occurs around 30-40 fm/c. From Fig. 2 it can be noted that this is also the time at which the average mean field energy drops drastically. For lower energies, the transition from the interacting to the freezed out system is not so sharp. However, even there one can determine that the average freeze-out time is around 40 fm/c [27].

In Fig. 16, we show the average and central densities of the colliding system as a function of time. The central density was determined in a radius of 2 fm around the center of mass, while for the average density the r.m.s radius of the colliding system was used. In Fig. 17, the ERAT values are given as the function of time. All of these figures confirm the above given freeze-out time of approx. 40 fm/c. We find the average density at the freeze-out time to be  $0.3\varrho_0$  for 400 AMeV and around  $0.5\varrho_0$  at 150 AMeV, in agreement with other

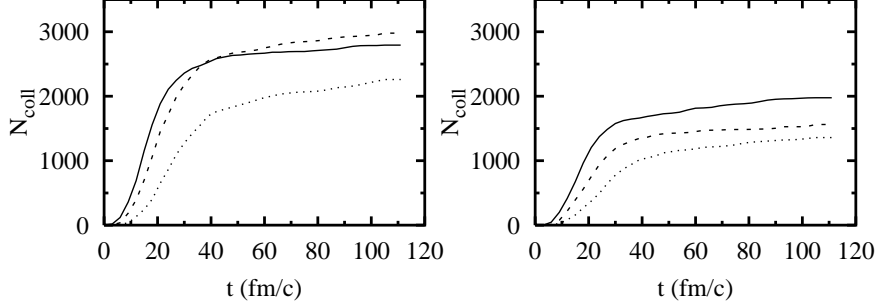


Fig. 15. Time evolution of the number of collisions at an impact parameter of  $b=0.5$  fm (left) and  $b=5.5$  fm (right) for 150 AMeV (dotted), 250 AMeV (dashed) and 400 AMeV (solid line).

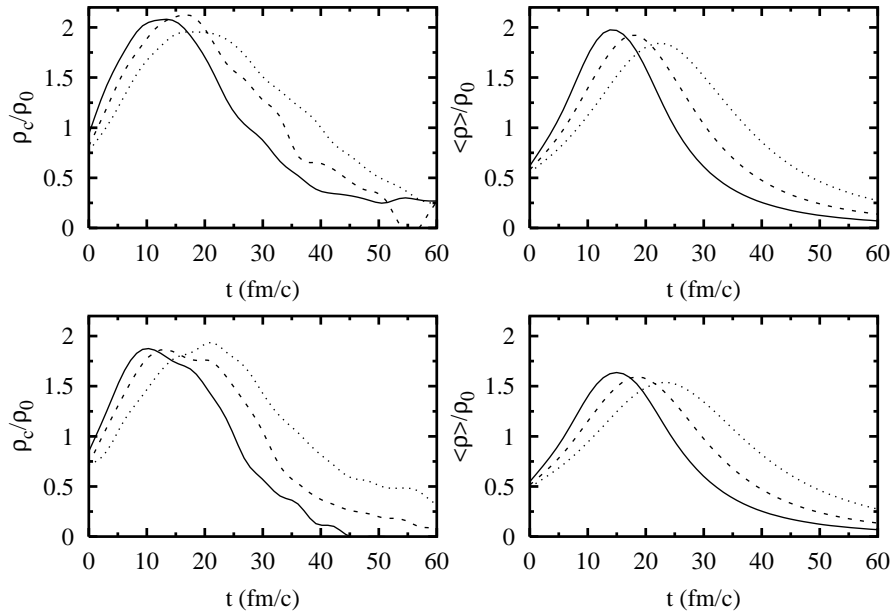


Fig. 16. Time evolution of the central (left) and average (right) density at an impact parameter of  $b=0.5$  fm (upper) and  $b=5.5$  fm (lower) for 150 AMeV (dotted), 250 AMeV (dashed) and 400 AMeV (solid line).

model predictions [25,27]

## 7 Conclusion

In this paper we derived a relativistically covariant Hamiltonian and the corresponding equations of motion starting from a Walecka type lagrangian with derivative coupling (Zimányi-Moszkowski lagrangian). The equations of motion can easily be solved in a QMD code for the approximation we introduced. We applied these equations to gold on gold collisions at 150, 250 and 400 AMeV, and compared our results with those of the FOPI experiment [1].

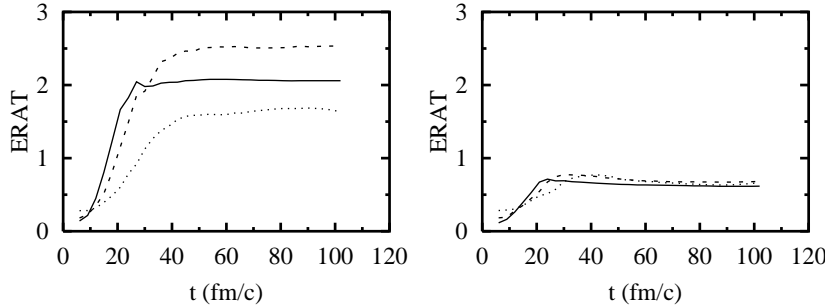


Fig. 17. Time evolution of the ERAT value at an impact parameter of  $b=0.5$  fm (left) and  $b=5.5$  fm (right) for 150 AMeV (dotted), 250 AMeV (dashed) and 400 AMeV (solid line).

We found that the experimental filtering criteria (ERAT200D) selects the very central events for 400 AMeV, and approximately central events for lower energies. The results obtained from our model are in agreement with most of the experimental observatories, however, the mean kinetic energies of large fragments are smaller than the measured ones.

The calculated IMF numbers are found to be close to the experimental results, but still lower. Furthermore, our calculations show that these numbers are rather insensitive to most details of the model, the only relevant quantity is the saturation density of the equation of state.

The model reproduces most of the experimental flow results. The fact that the mean flow velocities agree with the experimental ones for all three beam energies indicates, that the momentum dependence of the applied mean-field force is satisfactory. We would like to emphasize again that this momentum dependence is a result of the relativistic lagrangian and contains no additional parameters.

The freeze-out time for central collisions is between 30 and 50 fm/c, depending on the beam energy. The transition to the frozen stage is more pronounced for higher energies. The freeze-out density for central collisions is around third–half the nuclear matter saturation density depending on the beam energy, and smaller for higher energies.

We believe that the Zimányi-Moszkowski lagrangian, which assumes a derivative coupling between the scalar field and the nucleons, provides an adequate momentum dependent mean-field not only for nuclear matter where the adjustment of the coupling strengths to saturation density and binding energy provides also the proper momentum dependence, but also for heavy ion collisions where the proper momentum dependence is essential.

The energy is well conserved during the collision process: even in the case of 400 AMeV beam energy, the maximal deviation is less than 0.8 MeV per

particle. This shows that the individual nucleon-nucleon collision process and the effective mass is reasonably treated.

We found that the derived relativistically covariant Hamiltonian gives good results with the QMD code in the energy range of 150–400 AMeV. Since the approximations applied are still valid at 1 AGeV this model seems to be appropriate to study higher energy collisions, where particle production starts to be important. This work is in progress.

## Acknowledgments

One of the authors (J.N.) should like to express her thanks to Prof. W. Greiner and the University of Frankfurt and to Prof. Nörenberg and the GSI for their kind hospitality, during her visit to this institutions, where part of this work was done. Discussions with W. Reisdorf and A. Gobbi are highly acknowledged. We express our thanks to the FOPI group providing the experimental filter program. This work was partly supported by Hungarian OTKA grant T022931 and FKFP grant 0126/1997.

## References

- [1] W. Reisdorf *et al.*, Nucl. Phys. **A612** (1997) 493.
- [2] H. Feldmeier, J. Németh and G. Papp, APH Heavy Ion Physics **3** (1996) 71.
- [3] FOPI collaboration, Nucl. Phys. **A586** (1995) 755; M. Petrovici *et al.*, Phys. Rev. Lett. **74** (1995) 5001; S.C. Jeong *et al.*, Phys. Rev. Lett. **72** (1994) 3468; W.C. Hsi *et al.*, Phys. Rev. Lett. **73** (1994) 3367.
- [4] G.F. Bertsch and S. Das Gupta, Phys. Rep. **160** (1988) 189; W. Cassings, V. Metag, U. Mosel and K. Niita, Phys. Rep. **188** (1990) 363.
- [5] J. Aichelin, Prog. Nucl. Part. Phys. **30** (1991) 191; J. Aichelin, G. Peilert, A. Bohnet, A. Rosenhauer, H. Stöcker and W. Greiner, Phys. Rev. **C372** (1988) 451; J. Aichelin, Phys. Rep. **202** (1991) 233.
- [6] G. Peilert, H. Stöcker and W. Greiner, Rep. Prog. Phys. **57** (1994) 533; J. Konopka, Prog. Part. and Nucl. Phys. **30** (1993) 301; C. Hartnack *et al.*, Nucl. Phys. **A580** (1994) 643.
- [7] J. Boguta and A.R. Bodmer, Nucl. Phys. **A292** (1977) 413.
- [8] J. Zimányi and S.A. Moszkowski, Phys. Rev. **C42** (1990) 1416
- [9] H. Feldmeier, in “*Relativity in General*”, eds. J. Diaz Alonso and M. Lorente Paramo, (Editions Frontières 1994, ISBN 2-86332-168-4).

- [10] J.A. Wheeler and R.P. Feynman, Rev. Mod. Phys. **21** (1949) 425.
- [11] A. Ono, H. Horiuchi, T. Maruyama and A. Ohnishi, Phys. Rev. Lett. **68** (1992) 2898; Prog. Theor. Phys. **87** (1992) 1185.
- [12] H. Feldmeier; Nucl. Phys. **A515** (1990) 147; H. Feldmeier, K. Bieler and J. Schnack, Nucl. Phys. **A586** (1995) 493.
- [13] H. Feldmeier and J. Lindner, Z. Physik **A341** (1991) 83.
- [14] L. Bel and J. Martin, Ann. Inst. Henri Poincaré, A XXII (1975) 173; L. Bel and J. Martin, Phys. Rev. **D9** (1974) 2760.
- [15] J.D. Jackson, Classical Electrodynamics, (New York: John Wiley & Sons, Inc., 1962).
- [16] B.D. Serot and J.D. Walecka, Adv. Nucl. Phys. **16** (1986) 1.
- [17] J. Németh, C. Ngô, H. Ngô and L. De Paula, XX. International Workshop in Hirschegg (1992) p262.
- [18] L. De Paula, J. Németh, Sa Ben Hao, S. Leray, C. Ngô, S.R. Souza and Zheng Yu Heng, Phys. Lett. **B258** (1991) 251; S.R. Souza, L. De Paula, S. Leray, J. Németh, C. Ngô and H. Ngô, Nucl. Phys. **A571** (1994) 159.
- [19] J. Cugnon, T. Mizutani and J. Vandermeulen, Nucl. Phys. **A352** (1981) 505.
- [20] Gy. Wolf, G. Batko, W. Cassing, U. Mosel, K. Niita and M. Schäfer, Nucl. Phys. **A517** (1990) 615.
- [21] J. Németh and G. Papp, in “*Dynamical features of nuclei*”, p36; ed. by X. Vinas, World Scientific, 1994.
- [22] J. Németh, Heavy Ion Physics **5** (1997) 249.
- [23] H. A. Gustafsson et al., Phys. Rev. Lett. **52** (1984) 1590; H. H. Gutbrod, A. M. Poskanzer and H. G. Ritter, Rep. Prog. Phys. **52** (1989) 1267.
- [24] P. Danielewicz, Phys. Rev. **C51** (1995) 716; J. Konopka, H. Stöcker and W. Greiner, Proc. XXII. Hirschegg Workshop, Hirschegg, Austria 1994, p218.
- [25] W. Reisdorf, XXII. Hirschegg Workshop (1994) p93; W. Nörenberg and G. Papp, in “*Critical Phenomena and Collective Observables*”, ed. S. Costa, S. Albergo, A. Insola, C. Tuvé; World Scientific, 1996, Singapore, p. 377.
- [26] J. Németh and G. Papp, nucl-th/9711039.
- [27] G. Papp and W. Nörenberg, Heavy Ion Physics **1** (1995) 241; G. Papp, J. Németh and J.P. Bondorf, Phys. Lett. **B278** (1992) 7.